International Journal of Nanomedicine

Dovepress
open access to scientific and medical research

Open Access Full Text Article

ORIGINAL RESEARCH

Carbon Dots from *Paeoniae Radix Alba* Carbonisata: Hepatoprotective Effect

This article was published in the following Dove Press journal:
International Journal of Nanomedicine

Yusheng Zhao[1]
Yue Zhang[2]
Hui Kong[3]
Meiling Zhang[3]
Jinjun Cheng[3]
Jiashu Wu[3]
Huihua Qu[4]
Yan Zhao[3]

[1]School of Chinese Materia Medica, Beijing University of Chinese Medicine, Beijing 100029, People's Republic of China; [2]School of Life Sciences, Beijing University of Chinese Medicine, Beijing 100029, People's Republic of China; [3]School of Traditional Chinese Medicine, Beijing University of Chinese Medicine, Beijing 100029, People's Republic of China; [4]Centre of Scientific Experiment, Beijing University of Chinese Medicine, Beijing 100029, People's Republic of China

Introduction: The charcoal processed product of *Paeoniae Radix Alba* (PRA), PRA Carbonisata (PRAC), has long been used for its hepatoprotective effects. However, the material basis and mechanism of action of PRAC remain unclear.

Aim: To explore the hepatoprotective effects of *Paeoniae Radix Alba* Carbonisata-derived carbon dots (PRAC-CDs).

Methods: PRAC-CDs were characterized using transmission electron microscopy, high-resolution transmission electron microscopy, ultraviolet, fluorescence, Fourier transform infrared and X-ray photoelectron spectroscopy, X-ray diffraction, and high-performance liquid chromatography. The hepatoprotective effect of PRAC-CDs was evaluated and confirmed using the classic carbon tetrachloride acute liver injury model.

Results: PRAC-CDs averaged 1.0–2.4 nm in size and exhibited a quantum yield of 5.34% at a maximum excitation wavelength of 320 nm and emission at 411 nm. PRAC-CDs can reduce the ALT and AST levels of mice with carbon tetrachloride-induced acute liver injury and have a mitigating effect on the rise in TBA and TBIL. More interestingly, PRAC-CDs can significantly reduce MDA and increase SOD levels, demonstrating that PRAC-CDs can improve the body's ability to scavenge oxygen free radicals and inhibit free radical-induced liver cell lipid peroxidation, thereby preventing liver cell damage.

Conclusion: These results demonstrate the remarkable hepatoprotective effects of PRAC-CDs against carbon tetrachloride-induced acute liver injury, which provide new insights into potential biomedical and healthcare applications of CDs.

Keywords: *Paeoniae Radix Alba* carbonisata, carbon dots, hepatoprotective

Introduction

Carbon dots (CDs), an emerging nanomaterial with particle sizes under 10 nm, have many advantageous properties, including high photostability, low toxicity, fine biocompatibility, and good water dispersity.[1,2] The advantages of unique CDs are already being utilized for a number of potential biomedical applications, such as in biological imaging,[3,4] drug delivery,[5,6] and biosensors.[7,8] In recent years, the application of nanomedicine in the treatment of diseases has received widespread attention and has shown great clinical potential.[9]

CDs extracted from charcoal drugs are considered to be extracted from natural products, similar to the current process of preparing CDs. High-temperature carbonization is a key step in the preparation of traditional Chinese medicine (TCM) charcoal formulations. Previous studies have shown that carbon dots from *Pollen Typhae Carbonisata*[10] and *Cirsium Setosum Carbonisata*[11] effectively decreased the activated partial thromboplastin time and increased fibrinogen levels, indicating

Correspondence: Huihua Qu
Tel +86 10 6428 6705
Fax +86 10 6428 6821
Email quhuihuadr@163.com

Yan Zhao
Tel +86 10 6428 6705
Fax +86 10 6428 6821
Email zhaoyandr@163.com

that carbon dots have the ability to activate haemostasis. Wang et al[12] used a high-temperature pyrolysis method to formulate CDs from *Aurantii Fructus Immaturus Carbonisata* and proved that they have antihyperuricaemic and anti-gouty arthritis effects. The inherent biological activity and potential pharmacological effects of CDs have not yet attracted sufficient attention and are worthy of further study.

Paeoniae Radix Alba (PRA), the dried roots of *Paeonia lactiflora Pall*, is a TCM widely used in China. PRA was first recorded as a drug in *Sheng Nong's Herbal Classic*, which was written more than 2000 years ago. The charcoal processed product of PRA, PRAC Carbonisata (PRAC), has long been used for its hepatoprotective effects. However, the material basis and mechanism of action of PRAC remain unclear. In this study, we focus on the carbon dots generated by charcoal processing from the perspective of materials science.

Liver injury is defined as acute liver dysfunction caused by viral infection, liver toxicity, toxic substances or hepatic ischaemia-reperfusion.[13] The liver is the main organ involved in drug metabolism in the body, so chemical liver injury is very common. Commonly used drugs and laboratory chemicals such as paracetamol, amine sulfate and alcohol can damage the liver by producing reactive oxygen species.[14] However, the current treatment for chemical liver injury is not adequate, and a safe and effective drug is still urgently needed.

In this study, we used electron microscopy and optical instruments to discover novel carbon dots, which we named PARC-CDs. To study their hepatoprotective effects, we established a modified liver injury model that uses carbon tetrachloride to induce liver injury in mice. We evaluated the hepatoprotective effects of different doses of PARC-CDs.

Materials and Methods

Chemicals

PRA was purchased from Beijing Qian Baicao Co., Ltd (Beijing, China), and PRAC was prepared in our laboratory. Analytical-grade chemical reagents were obtained from Sinopharm Chemical Reagents Beijing (Beijing, China). Bifendate was purchased from Beijing Xiehe Pharmaceutical Factory. Dialysis bags of 1000 Da molecular weight cut-off was purchased from Beijing Ruida Henghui Technology Development Co., Ltd. (Beijing, China). Cell counting kit-8 (CCK-8) was obtained from Dojindo Molecular Technologies, Inc., (Kumamoto, Japan). CA4-PRO automatic biochemical analyser was purchased from Beckman, USA. A malondialdehyde (MDA) kit and superoxide dismutase (SOD) kit were purchased from Nanjing Jiancheng Bioengineering Institute. All the experiments were performed using deionised water (DW).

Animals

All the experimental procedures were performed in accordance with the Regulations for the Administration of Affairs Concerning Experimental Animals approved by the State Council of People's Republic of China. The animal experimental design and protocols used in this study were approved by the Ethics Review Committee for Animal Experimentation at the Beijing University of Chinese Medicine. Mouse monocyte macrophage RAW 264.7 cells were purchased with Peking Union Cell Bank (Beijing, China). Male mus musculus (weighing 32.0 ± 1.0 g) were purchased from Beijing Jinmuyang Liability Co., Ltd. (Beijing, China) and kept in a well-ventilated room at 24.0 ± 1.0°C with 55–65% relative humidity and a 12 h light: dark cycle. The animals were given water and food ad libitum.

Preparation of PARC-CDs

First, 120 g PAR was placed in crucibles, covered with aluminium foil paper and the lid was closed to form a tight seal, then calcined in a muffle furnace (TL0612, Beijing Zhong Ke Anbo Technology Co., Ltd., China) for 1 h at 350°C to produce PARC and cooled to room temperature. After crushed into fine powder, the PARC was dissolved in DW and boiled two times for 1 hour. After filtered the residue with filter paper, the solution was concentrated in 50mL and then dialyzed using a 1.0 kDa dialysis membrane for 72 h. Finally, the water extract containing PARC-CDs was stored at 4°C until further experiments. The preparation process for PARC-CDs is shown in Figure 1.

Fingerprint Analysis of PARC-CDs

The components of the aqueous PRA solution obtained at 350°C and the ethanol PRA extract were measured using an Agilent 1260 series high-performance liquid chromatography (HPLC) instrument (Agilent, Waldbronn, Germany). A C18 column (250 mm × 4.6 mm, Orochem, IL, USA) packed with 5 mm octadecyl-bonded silica (C18) was used for PRAC-CDs separation. All samples were filtered with a 0.22 μm cellulose membrane (Jin Teng, Tianjin, China) prior to use. Mobile phases A and B were 0.05% phosphoric acid solution and acetonitrile, respectively. As previously

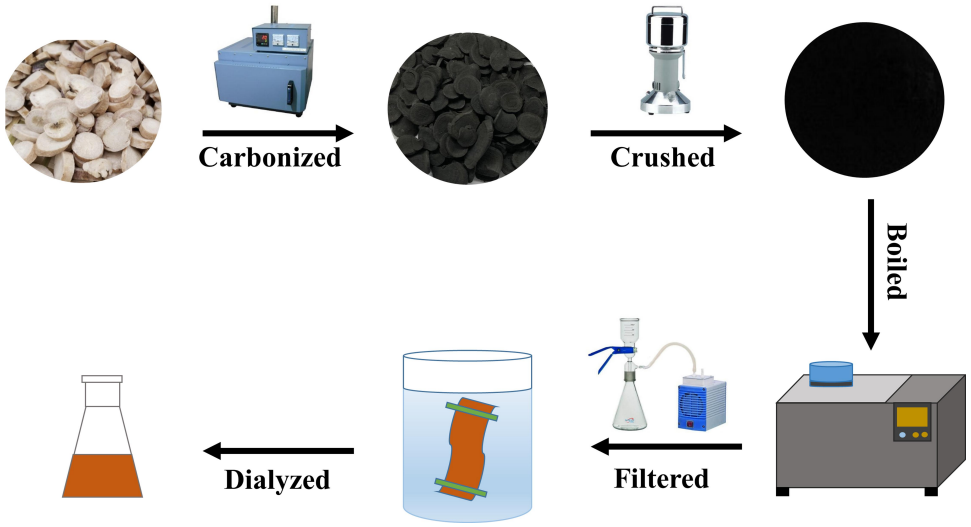

Figure 1 The flowchart for the preparation process of PARC-CDs.

reported,[15] a modified gradient elution programme was utilized at a flow rate of 1 mL/min as follows: 0–10 min, 8%-18% B; 10–25 min, 18–20% B; 25–30 min, 20% B; 30–40 min, 20–25% B; 40–55 min, 25–40% B; 55–60 min, 40–45% B; 60–70 min, 45–8% B. The column temperature was 30°C, and the injected sample quantity was maintained at 15 μL. The detection wavelength was set at 230 nm.

Characterisation of PARC-CDs

The morphology, particle size distribution and microstructure of PARC-CDs were characterized by TEM (Tecnai G220; FEI Company, USA) at an accelerating voltage of 100 kV. Atomic lattice fringes and other structural details were observed by HRTEM (JEN-1230; Japan Electron Optics Laboratory; Japan). The spectral properties of the CDs were analysed using an ultraviolet spectrophotometer (CECIL, Cambridge, UK) and fluorescence spectrophotometer (F-4500, Tokyo, Japan). In addition, FTIR spectroscopy (Thermo Fisher, Fremont, CA, USA) was used to identify the distribution of functional organic groups on the surface of PARC-CDs within 4000–400 cm^{-1}. The surface and elemental composition of the CDs were examined using X-ray photoelectron spectroscopy (XPS) (ESCALAB 250Xi; Thermo Fisher Scientific, USA) with a mono X-ray source Al Kα excitation (1,486.6 eV). XRD (D8-Advanced X-ray diffractometer, Bruker AXS, Karlsruhe, Germany) was performed with Cu K-alpha radiation.

Quantum Yield of PARC-CDs

Quantum yield (QY) was measured with quinine sulfate as the reference (%QY was 54 in 0.1 M sulphuric acid [H_2SO_4] solution). In order to minimize the reabsorption effect, A_C and A_R were guaranteed below 0.05. QY of the PARC-CDs is calculated according to the following formula.[16,17]

$$Q_{CDs} = Q_R \times \frac{I_{CDs}}{I_R} \times \frac{A_R}{A_{CDs}} \times \frac{\eta_{CDs}^2}{\eta_R^2}$$

Where Q represents fluorescence quantum yield, I is the measured integrated emission intensity, A and η represent the 320 nm absorption value and the refractive index of the solvent. "CDs" and "R" represent the PARC-CDs and the standard, respectively.

Cell Viability Assay

Safety is one of the first factors considered for potential clinical applications. Because drug toxicity is mostly related to the induction of bodily inflammation and oxidative stress, macrophages play an important role in various immune inflammation processes.[18] Macrophages are currently one of the cell lines commonly used to determine drug toxicity. The cytotoxicity of the PARC-CDs was evaluated in RAW 264.7 cells using a CCK-8 assay.[19] RAW 264.7 cells were cultured in DMEM supplemented with 20% foetal bovine serum at 37°C in a humidified 5% CO2 atmosphere. First, the cells were spread on a 96-well plate at a density of 1×105 cells per well and incubated for 24 hours. Then, after the original medium in each well was discarded, 100 μL of different concentrations of PARC-CDs were added to the designated wells, and DMEM was added to the control group. After the plate was washed three times with PBS, 10 μL of CCK-8 reagent was added to each well for an additional 4 h of incubation.

A microplate reader (Biotek, Vermont, USA) was used to measure the absorbance of each well at 450 nm. The cell viability was calculated according to the following formula:

$$\text{Cell Viability (\% of control)} = \frac{\text{Ae} - \text{Ab}}{\text{Ac} - \text{Ab}} \times 100$$

where Ae, Ab and Ac represent the absorbance of the experimental, blank and control groups, respectively, at 450 nm.

Models of Acute Liver Injury and Drug Treatment

The acute liver injury model was established as previously reported.[13] Male mus musculus (n = 48) were randomized into the following six groups (n = 8 in each) and treated as indicated: the negative control group (normal saline [NS] intraperitoneal injection), the model group (intraperitoneal injection), the positive control group (2.25 mg/kg [Bifendate] subcutaneous injection) and the high-, medium- and low-dose PARC-CDs groups (6.16, 3.08 and 1.54 mg/kg, respectively, intraperitoneal injection). The normal group and the model group were given equal volumes of normal saline, and all the PARC-CDs groups underwent intragastric administration for 7 days. Two hours after the final administration, all of the groups were injected intraperitoneally with the prepared carbon tetrachloride oil solution (10 mL/kg), except for the negative control group, which received an intraperitoneal injection of an equal volume of corn oil.

Determination of Biochemical Indices

After twelve hours, mice were anaesthetized with 4% chloral hydrate (0.40 g/kg). Retro-orbital blood samples were collected and centrifuged at 750 × g for 15 min to isolate the supernatant. Those samples were analysed using a serum analyser (XI-800, Sismecon Co., Ltd, Japan). First, the changes in alanine transaminase (ALT) and aspartate aminotransferase (AST) activity in the sera were determined using an automatic biochemical analyser, and then the levels of total bile acids (TBA), total bilirubin (TBIL), and triglycerides (TG) were determined using an automatic biochemical analyser. Finally, changes in superoxide dismutase (SOD) and malondialdehyde (MDA) levels in liver homogenates were measured according to the kit instructions, and the mechanism of PARC-CDs-driven protection from liver injury was studied in detail via transaminase, choleretic, and liver cell membrane lipid peroxidation levels.

Statistical Analysis

The statistical analysis was carried out using the computer program SPSS (version 19.0, Chicago, IL). The non-normally distributed data were expressed as median values (with quartile ranges). The normally distributed data and homogeneous variances were expressed as the mean ± standard deviation. Multiple comparisons were performed using a one-way analysis of variance (ANOVA) followed by a least significant difference test. $p < 0.05$ and $p < 0.01$ indicated statistically significant differences.

Results

High-Performance Liquid Chromatography Data Analysis

Figure 2A shows the chromatogram of the ethanol extract of PRA. A series of peaks for small-molecule compounds were observed, and a specific peak corresponding to the index component, paeoniflorin, was present. As shown in Figure 2B, no significant peaks were observed in the PRAC-CDs solution under the same conditions. It is obvious that the small molecular components that existed in PRA had disappeared in the PRAC-CD solution after charcoal processing and dialysis.

Characterisation of PRAC-CDs

The TEM images of the PRAC-CDs revealed that the CDs were nearly spherical and separated from each other without apparent aggregation (Figure 3A). The size distribution of the PRAC-CDs was in the range of 1.0–2.4 nm and conformed to normal distribution characteristics, as determined by the statistical analysis of more than 100 particles by using ImageJ software. As shown in Figure 3D, the high-resolution TEM images showed well-resolved lattice fringes and a lattice spacing of 0.200 nm. These morphological proportions are consistent with previous reports.[20] Figure 3B shows that the XRD spectrum of PRAC-CDs had distinct diffraction peaks ($2\theta = 21.141°$), indicating that PRAC-CDs were composed of amorphous carbons arranged in a considerably random fashion,[21] and their atomic lattice fringes were calculated to be 0.205 nm, confirming the measurement results from the HRTEM images.

The luminescent properties of the PRAC-CDs were investigated next. The UV–Vis spectrum (Figure 3C) of

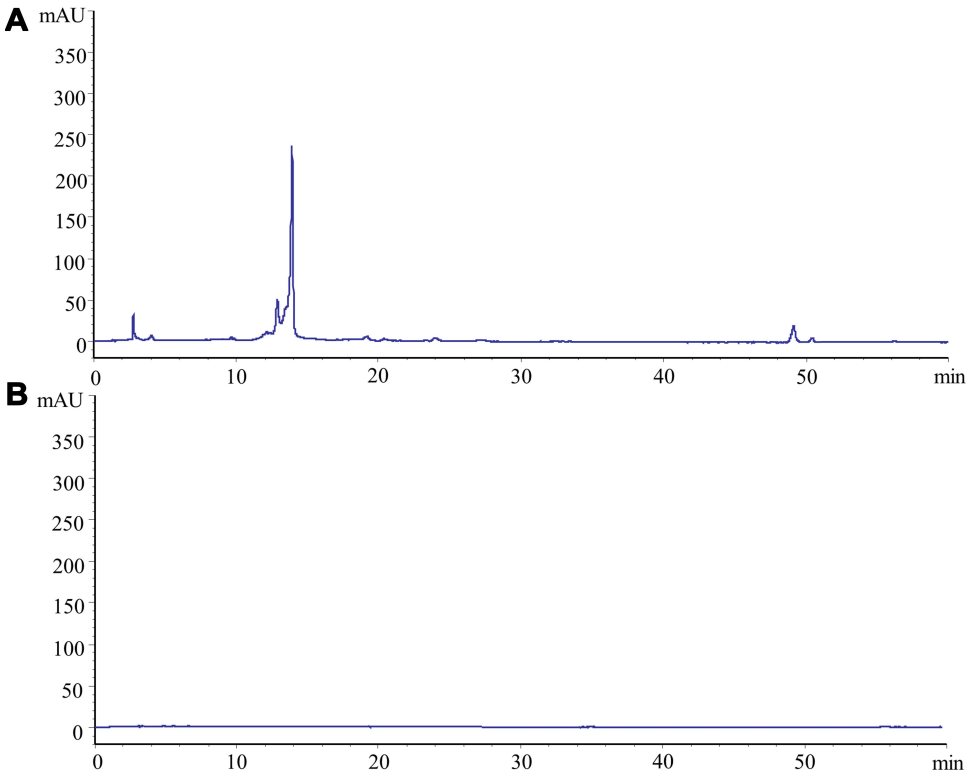

Figure 2 High-performance liquid chromatography (HPLC) fingerprints of (**A**) PRA (the dry root of *Paeonia lactiflora* Pall.) and (**B**) *Paeoniae Radix Alba Carbonisata.*

the aqueous PRAC-CDs solution exhibited a small absorption peak at 260 nm, which was attributed to the π–π* electron transition of the conjugated C=C bonds and aromatic sp^2 domains.[22] The fluorescence emission spectra showed the highest emission peak at 411 nm when excited at 320 nm, displayed in Figure 3E, and the QY of PRAC-CDs was calculated to be 5.34% using quinine sulfate as a reference. Fluorescence emission from carbon dots is due to the recombination of radiation between electrons and holes that are generated and trapped on the surface of the carbon dots. The different surface functional groups of carbon dots contribute to different emission states, resulting in excitation-dependent emission.[23] The surface chemical characteristics of the PRAC-CDs were analysed by FTIR spectroscopy (Figure 3F). The strong characteristic absorption at 3406 cm^{-1} indicated the existence of -O-H stretching vibrations. The absorption signals at 2928 cm^{-1} and 2856 cm^{-1} were attributed to –C–H stretching, which may occur because of the association of methyl or methylene groups with the aliphatic hydrocarbons present in PRAC-CDs. The intense peak at approximately 1564 cm^{-1} is identified as corresponding to C=O or O-N=O groups. On the one hand, this peak may be due to the presence of numerous double bond groups near the C=O bond, causing it to blue shift; on the other hand, the peak may be the characteristic O-N=O group stretching vibration peak. The peak at 1412 cm^{-1} is attributed to the stretching vibration peak of C-N. In addition, the peak at 1066 cm^{-1} is related to C-O-C bonds. The presence of these functional groups, including carbonyl, carboxyl, and hydroxyl groups, confers hydrophilicity and aqueous solubility to the PRAC-CDs.[24,25]

The surface composition and chemical environments of the PRAC-CDs were further studied by X-ray photoelectron spectroscopy (XPS). As shown in Figure 4A, peaks were evident at 295.18, 405.98 and 541.68 eV, indicating that the quantum point was composed mainly of C (68.21%), O (29.10%), and a small amount of N (2.69%).

The C1s spectrum (Figure 4B) was deconvoluted into three peaks at 284.8, 286.01, and 288.48 eV, corresponding to C-N, C=O, C-O carboxyl groups. The O1s spectrum (Figure 4C) was divided into two peaks at 531.65 and 532.75 eV, which were assigned to C–O and C=O, respectively. Furthermore, Figure 4D shows the N1s spectrum indicating the different chemical environments of C-N-C at 399.8 eV and N-H at 400.6 eV.[26,27] These results were consistent with the surface composition of PRAC-CDs as determined by FTIR analysis.

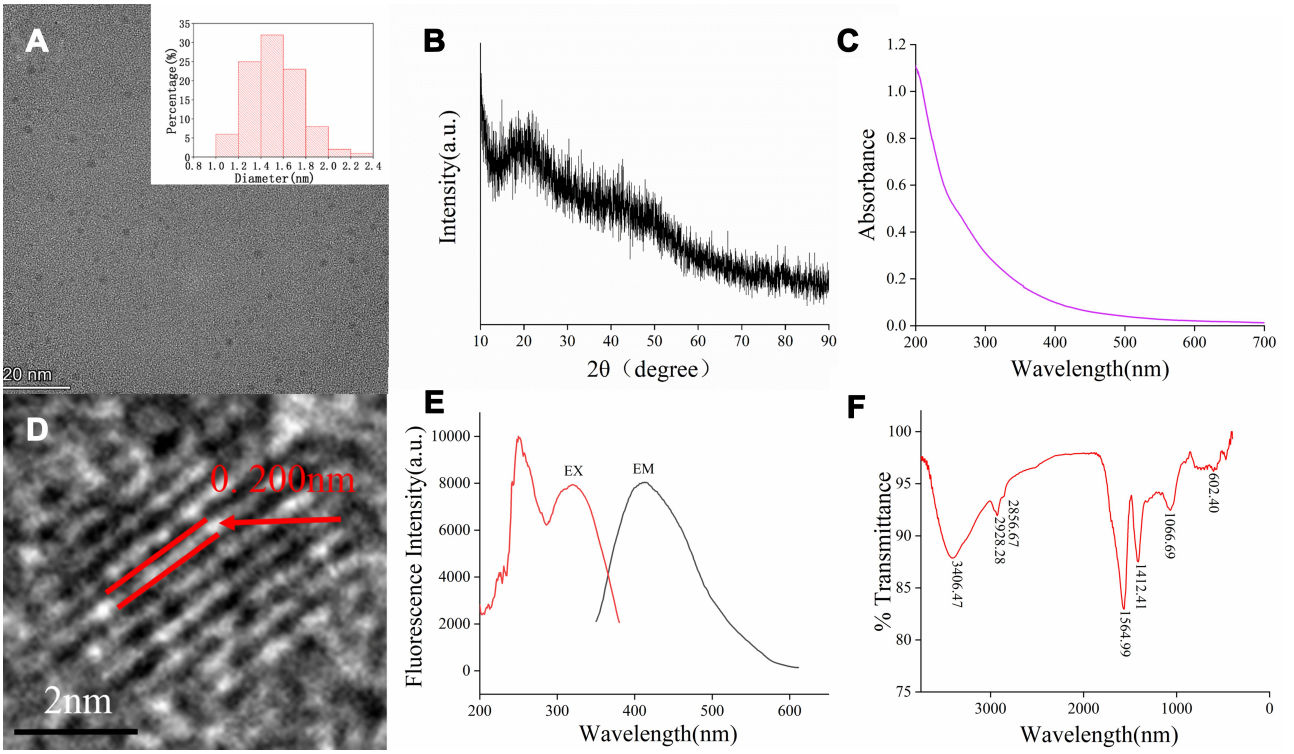

Figure 3 Characterization of PRAC-CDs: (**A**) Transmission electron microscopy (TEM) images of PRAC-CDs displaying ultrasmall particles and the TEM-determined size distribution of PRAC-CDs (upper right corner). (**B**) X-ray diffraction pattern. (**C**) Ultraviolet–visible spectrum. (**D**) High-resolution TEM image of PRAC-CDs. (**E**) Fluorescence spectrum. (**F**) Fourier transform infrared spectrum.

Cytotoxicity Detection

The safety of carbon dots has always been an important issue surrounding their biological application. To study the toxicity and safety of PRAC-CDs and, a CCK-8 assay was carried out to determine the cytotoxicity of PRAC-CDs to RAW264.7 cells. As shown in Figure 5, the concentration range studied was 29.30–7500 μg/mL, which has a positive effect on cell viability that shows a relatively stable trend. Based on the above experimental results, we can see that PRAC-CDs have low toxicity and a safety range of 29.30–7500 μg for promoting cell viability. This provides a potential reference value for future research and drug development for enhancing target cell viability.

The Effect of PRAC-CDs on the Transaminase and the Biliary Index

The mechanism of PRAC-CD-based protection from liver injury was evaluated by measuring transaminase activity and the biliary index (i.e., alanine transaminase (ALT), aspartate aminotransferase (AST), total bile acid (TBA), total bilirubin (TBIL), and triglyceride (TG) levels) in mice. As shown in Figure 6A and B, compared with those in the normal saline group (25.667 ± 2.887, 81.65 ± 6.576), the serum ALT and AST activities of mice in the model group (55.143 ± 4.860, 164.967 ± 14.016) were significantly elevated ($P < 0.01$), indicating that the model was functional. Compared with those in the model group, the serum ALT activity of mice in the bifendate group (27 ± 5.022) and high-, medium- and low-dose PRAC-CDs groups (29 ± 3.055, 34 ± 4.199, 34.667 ± 3.689, respectively) was significantly reduced ($P < 0.01$). Compared with that in the model group, the serum AST activity of mice in the bifendate group (104.2 ± 13.077) was significantly decreased ($P < 0. 01$), and that in the high-, medium- and low-dose PRAC-CDs groups (109.433 ± 20.220, 120.960 ± 18.073, 129.467 ±17.239, respectively) was decreased ($P < 0. 05$).

Figure 6C shows the effect of PRAC-CDs on the total bile acid levels (TBA) of mice with liver injury. Compared with those in the model group (3.48 ± 0.361), the serum TBA content in the bifendate group (2.203 ± 0.420) was decreased ($P < 0. 05$), and those of the high-, medium- and low-dose PRAC-CDs groups (2.720 ± 0.212, 2.925 ± 0.293, 3.043 ± 0.304, respectively) were significantly decreased ($P < 0. 01$). Figure 6D shows that serum total bilirubin (TBIL) levels in the bifendate (1.850 ± 0.222)

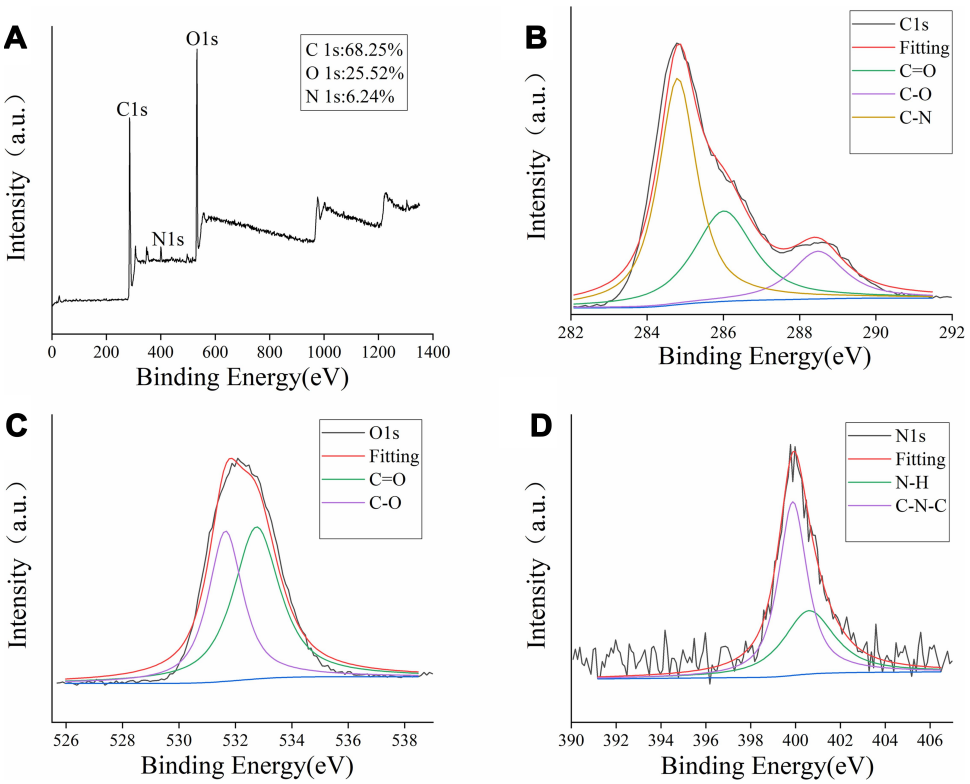

Figure 4 The surface composition and elemental analysis of the prepared PRAC-CDs by XPS. (**A**) X-ray photoelectron spectroscopic survey of PRAC-CDs. (**B**) C1s. (**C**) O1s and (**D**) N1s.

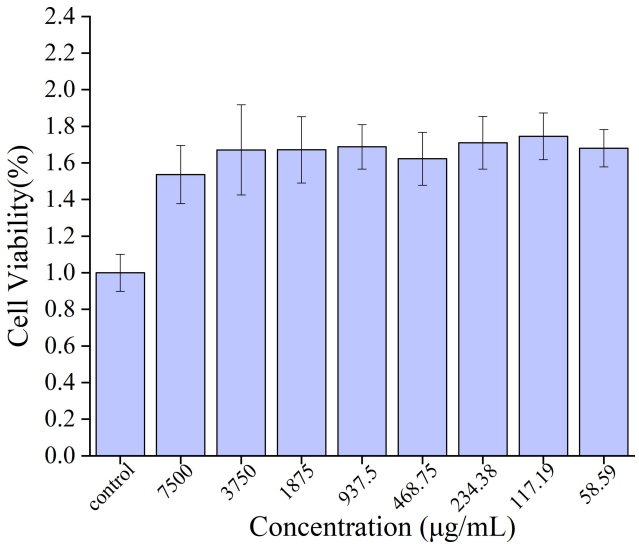

Figure 5 Effect of different concentrations of PRAC-CDs on the viability of RAW 264.7 cells.

and high-, medium- and low-dose PRAC-CDs groups (2.207 ± 0.173, 2.294 ± 0.217, 2.17 ± 0.092, respectively) were significantly decreased (P < 0. 01) compared to those of the model group (2.864 ± 0.231), indicating that PRAC-CDs have a stronger reducing effect on liver injury-induced increases in TBIL. Figure 6E shows the change in triglyceride (TG) levels, which were not significantly different among the five treatment groups.

The Effect of PRAC-CDs on SOD and MDA Levels in Liver Tissue

Superoxide dismutase (SOD) scavenges oxygen free radicals and thus can mitigate damage to liver cells. As shown in Figure 7A, compared with that in the normal saline group (149.70 ± 10.04 U/mg prot), the liver tissue SOD level in the model group (87.58 ± 9.23 U/mg prot) was significantly elevated (P < 0.01). Compared with those in the model group, the liver tissue SOD levels in the bifendate group (134.24 ± 14.76 U/mg prot) and high-, medium- and low-dose PRAC-CDs groups (133.93 ± 15.27 U/mg prot, 123.31 ± 9.80 U/mg prot, 109.98 ± 7.97 U/mg prot, respectively) were significantly increased (P < 0.01). MDA, to a certain extent, reflects the degree of liver injury. Figure 7B shows that the liver tissue MDA level in the model group (5.26 ± 0.51 nmol/mg prot) significantly differed from that in the normal saline group (2.55 ± 0.51 nmol/mg prot) (P < 0.01). Compared with those in the model group, the liver tissue MDA levels in the bifendate group (3.10 ± 0.56 nmol/mg

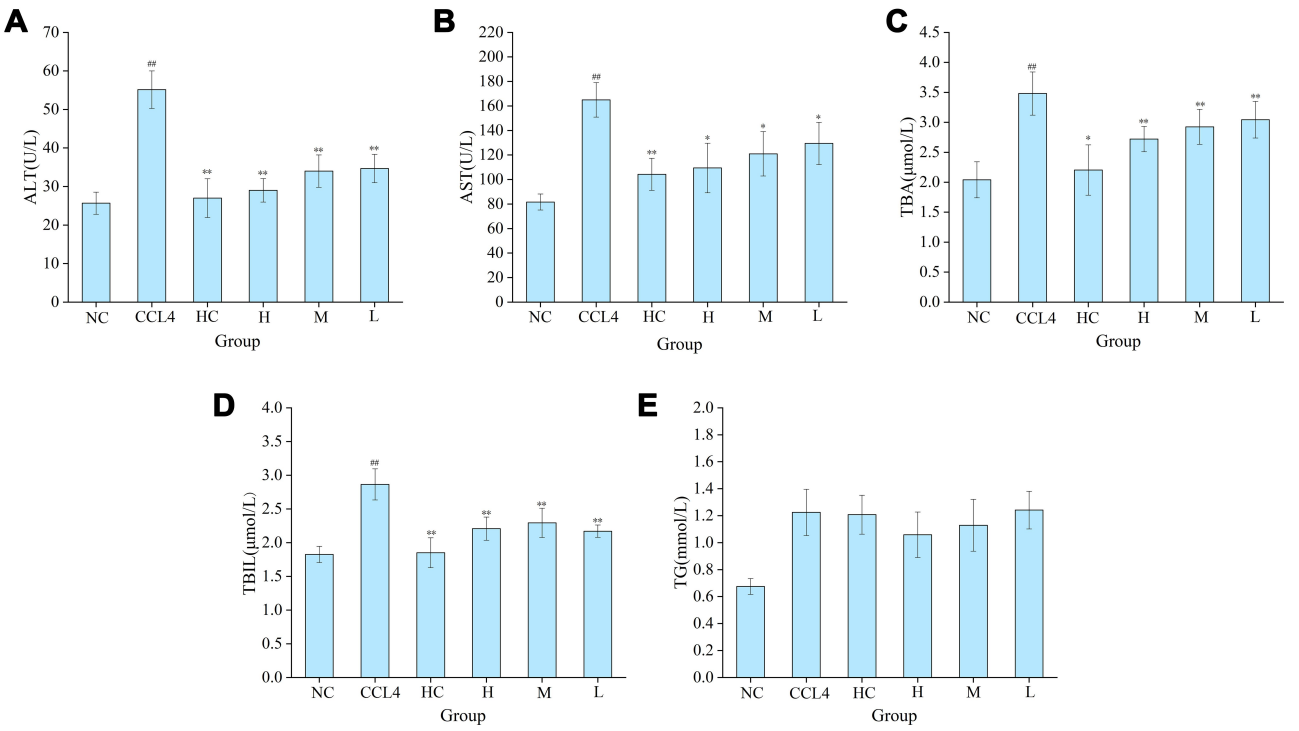

Figure 6 The effect of PRAC-CDs on transaminase levels and the biliary index. (**A**) Alanine aminotransferase (ALT), (**B**) Aspartate transferase (AST), (**C**) Total bile acid (TBA), (**D**) Total bilirubin (TBIL), and (**E**) Triglyceride (TG) levels. Analysis of mice treated with normal saline (NS), model (CCL_4), bifendate (BD), and high (H), medium (M), and low (L) doses of PRAC-CDs (6.16, 3.08 and 1.54 mg/kg, respectively). Significantly different compared with the control group at $^{\#\#}p < 0.01$, significantly different compared to the CCL_4 group (n = 8) at $^{**}p < 0.01$ and $^{*}p < 0.05$.

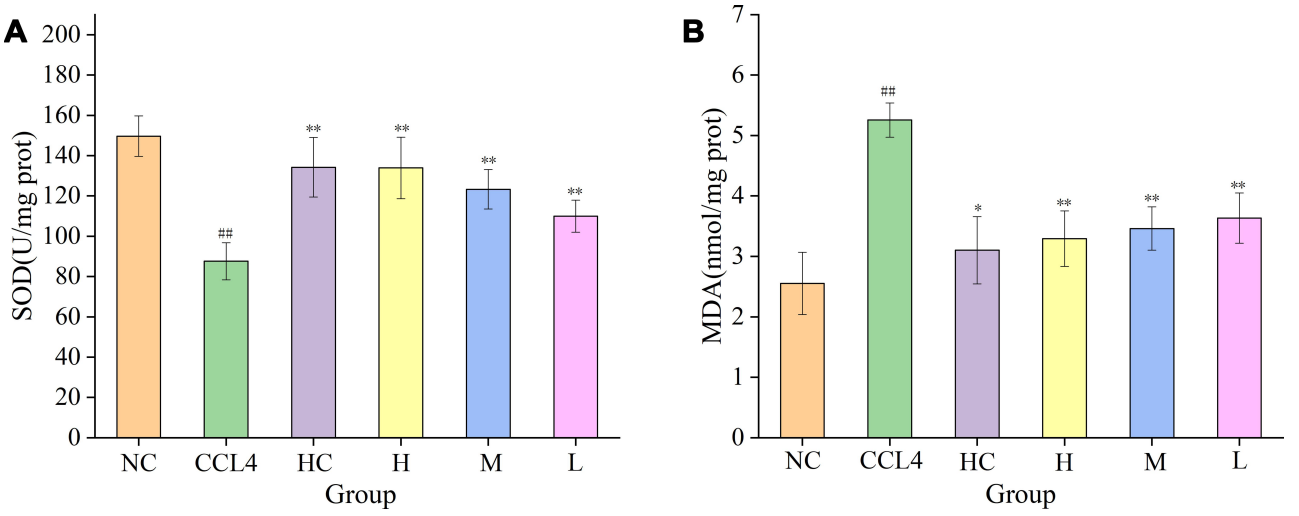

Figure 7 Effects on MDA and SOD levels in liver tissue of mice with CCl4-induced liver injury. (**A**) SOD and (**B**) MDA levels in mice treated with normal saline (NS), model (CCL4), bifendate (BD), and high (H), medium (M), and low (L) doses of PRAC-CDs (6.16, 3.08 and 1.54 mg/kg, respectively). Significantly different compared with the control group at $^{\#\#}p < 0.01$, significantly different compared to the CCL_4 group (n = 8) at $^{**}p < 0.01$ and $^{*}p < 0.05$.

prot) and high-, medium- and low-dose PRAC-CDs groups (3.29 ± 0.46 nmol/mg prot, 3.46 ± 0.36 nmol/mg prot, 3.63 ± 0.42 nmol/mg prot, respectively) were significantly reduced ($P < 0.01$). These results indicate that PRAC-CDs have a significant hepatoprotective effect.

Discussion

CDs are zero-dimensional carbon nanostructure materials with particle sizes usually below 10 nm that typically display excellent photoluminescence, biocompatibility, favourable chemical stability and good aqueous

solubility.[28,29] It is worth noting that the high-temperature pyrolysis preparation processes[30,31] for nanomaterial carbon dots and PRAC have similarities. This led us to change our thinking and consider introducing nano research technologies and methods into the study of carbon medicines in traditional Chinese medicine. It is worth referring to the preparation and characterization processes used for carbon dots to study the active ingredients in charcoal drugs. Based on this observation, the active ingredient in PARC may be the CDs produced during processing, which merits further study of its bioactivity. In this study, we characterized PRAC-CDs and demonstrated their hepatoprotective effect, thus allowing for the consideration of charcoal drugs as medicinal substances and their mechanism of action from a new perspective.

CDs have been reported in other charcoal drugs prepared at a high temperature, including *Junci Medulla Carbonisata, Pollen Typhae Carbonisata* and *Phellodendri Cortex Carbonisata*.[10,32,33] The size and morphology of PRAC-CDs were examined by employing the TEM technique and are similar to those previously reported for carbon dots.[34] The XPS and FTIR results show that the structure of PRAC-CDs comprises multiple functional groups, including carbonyl, carboxyl, and hydroxyl groups, and that the photoluminescence of CDs can be attributed to the multiphoton activation of various oxygen-containing functional groups.[35] Moreover, a comparison of the chemical compositions of PRA and PRAC-CDs was carried out to evaluate variations in their components. The main active components of PRA, including paeoniflorin and other small molecules, were observed in its HPLC fingerprint. In contrast, small molecular components were not found in the PRAC-CD solution following charcoal processing and dialysis, which excluded the potential confounding effects of small molecule compounds in hepatoprotection.

In this study, ALT and AST serum levels were elevated, indicating the successful recapitulation of the acute liver injury model, consistent with the literature.[36] Furthermore, all doses of PARC-CDs reduced the ALT and AST levels, especially the high dose. The metabolism of TBA and TBIL is dependent on liver function, and serum levels of both are proportional to the degree of liver damage. When compared with the model group, PARC-CDs administration can reduce the increase in TBA and TBIL to a certain extent, indicating that PARC-CDs can regulate the levels of TBA and TBIL and have liver-protective effects. TGs are mainly synthesized by the liver, and TG levels reflect another aspect of liver damage. Our experimental results show that while the PARC-CDs high-, medium- and low-dose groups have decreased TG levels compared with the model group, this decrease was not significant, indicating that PARC-CDs do not improve liver injury in mice by regulating TGs.

Lipid peroxidation is the main mechanism of CCL4-induced liver injury. When CCL4 enters the body of a mouse, a large number of free radicals are metabolized to produce a chain reaction of lipid peroxidation, ultimately leading to peroxidation of the lipid membrane.[37,38] The MDA content significantly increases with damage to membrane structure and function. MDA levels are often measured alongside SOD activity. The amount of MDA reflects the severity of the attack on the body's cells by free radicals, and the level of SOD activity indirectly reflects the body's ability to scavenge oxygen free radicals.[39] The results of this experiment show that treatment with high, medium and low doses of PARC-CDs can significantly reduce MDA levels and increase SOD levels, indicating that PARC-CDs can improve the body's ability to scavenge oxygen free radicals, inhibit free radical lipid peroxidation, and prevent liver cell damage. The mechanism by which PARC-CDs exert a hepatoprotective effect may prevent liver cell lipid peroxidation and thus mitigate damage to liver cells.

Conclusions

In summary, we succeeded in synthesizing and isolating novel CDs via simple pyrolysis of PAR. This study is the first to demonstrate that PARC-CDs possess remarkable hepatoprotective effects and that the underlying mechanism of that effect is associated with improving the body's ability to scavenge oxygen free radicals, prevent lipid peroxidation in liver cells and regulate the metabolism of bile acids and bilirubin. This study provides a new avenue for the research and development of therapeutic drugs for liver injury diseases and new insights into the exploration of the material basis of charcoal drugs.

Data Sharing Statement

The data that support the findings of this study are available from the corresponding author upon reasonable request.

Acknowledgments

This work was supported by the National Natural Science Foundation of China (81573573) and the Classical Prescription Basic Research Team of Beijing University of Chinese Medicine. The authors have no other relevant

affiliations or financial involvement with any organisation or entity with a financial interest in or financial conflict with the subject matter or materials discussed in the manuscript apart from those disclosed.

Disclosure

The authors report no conflicts of interest for this work.

References

1. Mishra V, Patil A, Thakur S, Kesharwani P. Carbon dots: emerging theranostic nanoarchitectures. *Drug Discov Today*. 2018;23(6):1219–1232. doi:10.1016/j.drudis.2018.01.006
2. Xu X, Ray R, Gu Y, et al. Electrophoretic analysis and purification of fluorescent single-walled carbon nanotube fragments. *J Am Chem Soc*. 2015;126(40):12736–12737. doi:10.1021/ja040082h
3. Sri S, Kumar R, Panda AK, et al. Highly biocompatible, fluorescence, and zwitterionic carbon dots as a novel approach for bioimaging applications in cancerous cells. *ACS Appl Mater Interfaces*. 2018;10(44):37835–37845. doi:10.1021/acsami.8b13217
4. He G, Xu M, Shu M, et al. Rapid solid-phase microwave synthesis of highly photoluminescent nitrogen-doped carbon dots for Fe^{3+}++ detection and cellular bioimaging. *Nanotechnology*. 2016;27(39):395706. doi:10.1088/0957-4484/27/39/395706
5. Kim J, Park J, Kim H, et al. Transfection and intracellular trafficking properties of carbon dot-gold nanoparticle molecular assembly conjugated with PEI-pDNA. *Biomaterials*. 2013;34(29):7168–7180. doi:10.1016/j.biomaterials.2013.05.072
6. Ye Q, Yan F, Kong D, et al. Chemical, A. B., constructing a fluorescent probe for specific detection of catechol based on 4-carboxyphenylboronic acid-functionalized carbon dots. *Sens Actuators B Chem*. 2012;51:712–720. doi:10.1016/j.snb.2017.03.081
7. Jana J, Ganguly GM, Das B, et al. One pot synthesis of intriguing fluorescent carbon dots for sensing and live cell imaging. *Talanta*. 2016;150:253–264. doi:10.1016/j.talanta.2015.12.047
8. Wang Y, Lu L, Peng H, et al. Multi-doped carbon dots with ratiometric pH sensing properties for monitoring enzyme catalytic reactions. *Chem Commun*. 2016;150(59):9247–9250. doi:10.1039/C6CC02874H
9. Min Y, Caster J, Eblan M, et al. Clinical translation of nanomedicine. *Chem Rev*. 2015;115(19):11147–11190. doi:10.1021/acs.chemrev.5b00116
10. Yan X, Zhao Y, Luo J, et al. Hemostatic bioactivity of novel pollen typhae carbonisata-derived carbon quantum dots. *J Nanobiotechnology*. 2017;15(1):60. doi:10.1186/s12951-017-0296-z
11. Luo J, Zhang M, Cheng J, et al. Hemostatic effect of novel carbon dots derived from Cirsium setosum Carbonisata. *RSC Adv*. 2018;8(66):37707–37714. doi:10.1039/C8RA06340K
12. Wang S, Zhang Y, Kong H, et al. Antihyperuricemic and anti-gouty arthritis activities of Aurantii fructus immaturus carbonisata-derived carbon dots. *Nanomedicine (Lond)*. 2019;14(22):2925–2939. doi:10.2217/nnm-2019-0255
13. Xu G, Han X, Yuan G, et al. Screening for the protective effect target of deproteinized extract of calf blood and its mechanisms in mice with CCl4-induced acute liver injury. *PLoS One*. 2017;12(7):e0180899. doi:10.1371/journal.pone.0180899
14. Ma J-Q, Li Z, Xie W, et al. Quercetin protects mouse liver against CCl4-induced inflammation by the TLR2/4 and MAPK/NF-κB pathway. *Int Immunopharmacol*. 2015;28(1):531–539. doi:10.1016/j.intimp.2015.06.036
15. Liu J, Chen L, Fan C, et al. Qualitative and quantitative analysis of major constituents of Paeoniae Radix Alba and Paeoniae Radix Rubra by HPLC-DAD-Q-TOF-MS/MS. *Zhongguo Zhong Yao*. 2015;40(9):1762–1770.
16. Ding C, Cao X, Zhang C, et al. Rare earth ions enhanced near infrared fluorescence of Ag2S quantum dots for the detection of fluoride ions in living cells. *Nanoscale*. 2017;9(37):14031–14038. doi:10.1039/C7NR04436D
17. Yang L, Jiang W, Qiu L, et al. One pot synthesis of highly luminescent polyethylene glycol anchored carbon dots functionalized with a nuclear localization signal peptide for cell nucleus imaging. *Nanoscale*. 2015;7(14):6104–6113. doi:10.1039/C5NR01080B
18. Jia P, Yu L, Tao C, et al. Chitosan oligosaccharides protect nucleus pulposus cells from hydrogen peroxide-induced apoptosis in a rat experimental model. *Biomed Pharmacother*. 2017;93:807–815. doi:10.1016/j.biopha.2017.06.101
19. Zhao G, Hu C, Xue Y, et al. In vitro evaluation of chitosan-coated liposome containing both coenzyme Q10 and alpha-lipoic acid: cytotoxicity, antioxidant activity, and antimicrobial activity. *J Cosmet Dermatol*. 2018;17(2):258–262. doi:10.1111/jocd.12369
20. Wang L, Bi Y, Hou J, et al. Facile, green and clean one-step synthesis of carbon dots from wool: application as a sensor for glyphosate detection based on the inner filter effect. *Talanta*. 2016;160:268. doi:10.1016/j.talanta.2016.07.020
21. Zhu C, Zhai J, Dong S, et al. Bifunctional fluorescent carbon nanodots: green synthesis via soy milk and application as metal-free electrocatalysts for oxygen reduction. *Chem Commun*. 2012;48(75):9367–9369. doi:10.1039/c2cc33844k
22. Melvin R, Mark G, Nichaphat T, et al. Highly fluorescent carbon dots from enokitake mushroom as multi-faceted optical nanomaterials for Cr^{6+} and VOC detection and imaging applications. *Appl Surf Sci*. 2018;453:192–203. doi:10.1016/j.apsusc.2018.04.199
23. Sharma V, Saini A, Mobin S, et al. Multicolour fluorescent carbon nanoparticle probes for live cell imaging and dual palladium and mercury sensors. *J Mater Chem B*. 2016;4(14):2466–2476. doi:10.1039/C6TB00238B
24. Qu S, Wang X, Lu Q, et al. A biocompatible fluorescent ink based on water-soluble luminescent carbon nanodots. *Angew Chem Int Ed Engl*. 2012;51(49):12215–12218. doi:10.1002/anie.201206791
25. Mewada A, Pandey S, Shinde S, et al. Green synthesis of biocompatible carbon dots using aqueous extract of Trapa bispinosa peel. *Mater Sci Eng C*. 2013;33(5):2914–2917. doi:10.1016/j.msec.2013.03.018
26. Li Y, Li S, Wang Y, et al. Electrochemical synthesis of phosphorus-doped graphene quantum dots for free radical scavenging. *Phys Chem Chem Phys*. 2017;19(18):11631–11638. doi:10.1039/C6CP06377B
27. Jie S, Shang S, Chen X, et al. Highly fluorescent N, S-co-doped carbon dots and their potential applications as antioxidants and sensitive probes for Cr (VI) detection. *Sens Actuators*. 2017;b248(sep):92–100.
28. Li Y, Zhao Y, Cheng H, et al. Nitrogen-doped graphene quantum dots with oxygen-rich functional groups. *J Am Chem Soc*. 2012;134(1):15–18. doi:10.1021/ja206030c
29. Shen J, Zhu Y, Yang X, et al. Graphene quantum dots: emergent nanolights for bioimaging, sensors, catalysis and photovoltaic devices. *Chem Commun (Camb)*. 2012;48(31):3686–3699. doi:10.1039/c2cc00110a
30. Lin P, Hsieh C, Kung M, et al. Eco-friendly synthesis of shrimp egg-derived carbon dots for fluorescent bioimaging. *J Biotechnol*. 2014;189:114–119. doi:10.1016/j.jbiotec.2014.08.043
31. Tan X, Romainor A, Chin S, et al. Carbon dots production via pyrolysis of sago waste as potential probe for metal ions sensing. *J Anal Appl Pyrolysis*. 2014;105(jan.):157–165. doi:10.1016/j.jaap.2013.11.001
32. Cheng J, Zhang M, Sun Z, et al. Hemostatic and hepatoprotective bioactivity of Junci Medulla carbonisata-derived carbon dots. *Nanomedicine (Lond)*. 2019;14(4):431–446. doi:10.2217/nnm-2018-0285
33. Liu X, Wang Y, Yan X, et al. Novel Phellodendri Cortex (Huang Bo)-derived carbon dots and their hemostatic effect. *Nanomedicine*. 2018;nnm-2017-0297.

34. Yang Y, Wang X, Liao G, et al. iRGD-decorated red shift emissive carbon nanodots for tumor targeting fluorescence imaging. *J Colloid Interface Sci*. 2018;509:515–521. doi:10.1016/j.jcis.2017.09.007
35. Wang Z, Liu J, Wang W, et al. Photoluminescent carbon quantum dot grafted silica nanoparticles directly synthesized from rice husk biomass. *J Mater Chem B*. 2017;5(24):4679–4689. doi:10.1039/C7TB00811B
36. Domitrovi R, Jakovac H, Marchesi V, et al. Differential hepatoprotective mechanisms of rutin and quercetin in CCl4-intoxicated BALB/cN mice. *Acta Pharmacol Sin*. 2012;33(10):1260–1270. doi:10.1038/aps.2012.62
37. Guo Y, Liang X, Meng M, et al. Hepatoprotective effects of Yulangsan flavone against carbon tetrachloride (CCl 4)-induced hepatic fibrosis in rats. *Phytomedicine*. 2017;33:28–35. doi:10.1016/j.phymed.2017.07.005
38. Fathy S, Drees E. Protective effects of Egyptian cloudy apple juice and apple peel extract on lipid peroxidation, antioxidant enzymes and inflammatory status in diabetic rat pancreas. *BMC Complement Altern Med*. 2015;16(1):8. doi:10.1186/s12906-015-0957-0
39. Jia R, Cao L, Du J, et al. Effects of carbon tetrachloride on oxidative stress, inflammatory response and hepatocyte apoptosis in common carp (Cyprinus carpio). *Aquat Toxicol*. 2014;152:11–19. doi:10.1016/j.aquatox.2014.02.014